

# A METHOD FOR NONLINEAR MODAL ANALYSIS AND SYNTHESIS: APPLICATION TO HARMONICALLY FORCED AND SELF-EXCITED MECHANICAL SYSTEMS

Malte Krack<sup>1,\*</sup>, Lars Panning-von Scheidt<sup>1</sup>, Jörg Wallaschek<sup>1</sup>

---

## Abstract

*The recently developed generalized Fourier-Galerkin method is complemented by a numerical continuation with respect to the kinetic energy, which extends the framework to the investigation of modal interactions resulting in folds of the nonlinear modes. In order to enhance the practicability regarding the investigation of complex large-scale systems, it is proposed to provide analytical gradients and exploit sparsity of the nonlinear part of the governing algebraic equations. A novel reduced order model (ROM) is developed for those regimes where internal resonances are absent. The approach allows for an accurate approximation of the multi-harmonic content of the resonant mode and accounts for the contributions of the off-resonant modes in their linearized forms. The ROM facilitates the efficient analysis of self-excited limit cycle oscillations, frequency response functions and the direct tracing of forced resonances. The ROM is equipped with a large parameter space including parameters associated with linear damping and near-resonant harmonic forcing terms. An important objective of this paper is to demonstrate the broad applicability of the proposed overall methodology. This is achieved by selected numerical examples including finite element models of structures with strongly nonlinear, non-conservative contact constraints.*

**Keywords:** nonlinear modal analysis, nonlinear modal synthesis, harmonic

---

\*Corresponding author

Email address: [krack@ila.uni-stuttgart.de](mailto:krack@ila.uni-stuttgart.de) (Malte Krack)

## 1. Introduction

Akin to its linear counterpart, nonlinear modal analysis is particularly suited for the analysis of dynamical systems. Modal analysis facilitates understanding of the energy-dependent system behavior in nonlinear systems regarding eigenfrequencies, modal damping, stiffening/softening characteristics, localization effects and internal resonances. The concept of nonlinear modes dates back to Rosenberg [1] and the interested reader is referred to [2, 3] for a good overview on various concepts and theories. Despite the fact that superposition and orthogonality conditions are not valid in the nonlinear case, nonlinear modes have been widely used for the approximate synthesis of forced vibrations [4, 5, 6, 7, 8].

In spite of their opportunities for qualitative and quantitative analysis of nonlinear systems, methods related to nonlinear modes are seldom applied to industrial problems. In the authors' opinion, the reasons are that most methods are restricted to smooth and conservative nonlinearities and rarely proved to cope with systems featuring many degrees of freedom (DOFs) such as large scale finite element models of typical industrial applications.

Several methods have been developed for analytical and numerical calculation of nonlinear modes in the past. We will focus on those methods which are well-suited for systems with generic and strong nonlinearities. Perturbation techniques such as the normal form approach [9] and the method of multiple scales [10] are not considered since they are restricted to small degree polynomial nonlinearities.

A method of broad applicability is the invariant manifold approach, as proposed in [11, 12, 13, 14, 15]. It is based on the invariance property of certain periodic motions of the system, i. e. a nonlinear mode is defined as an invariant relationship (manifold) between several master coordinates and the remaining

coordinates of the system. This manifold can be governed by partial differential equations arising from the substitution of the manifold into the state form of the equations of motion. For the solution of the governing equations, asymptotic expansions were originally employed [11, 15] and later a more general Galerkin ansatz was developed [16] to increase the accuracy of this approach. The invariant manifold approach was extended to account for the effect of harmonic excitation [13] and viscous damping [15]. Various systems have been studied, including piecewise linear systems [17] and systems with internally resonant nonlinear modes [14]. However, in these investigations, the focus of application was clearly set on small-scale systems with conservative nonlinearities.

Another class of methods for the determination of the modal properties of nonlinear systems is based on parameter identification, see e. g. [6, 7, 18]. Response data, obtained either by simulation or measurement, is gathered and modal parameters are identified by fitting original response data to data from nonlinear modal synthesis. An important subclass of parameter identification methods is the so called force appropriation, where the objective is to extract modal properties from the resonance reached by suitably adjusting the forcing parameters [19, 20, 21]. The weak point of these strategies is clearly their signal-dependent nature and the fact that the modal parameters are typically extracted from a forced rather than from an autonomous system. Moreover, further numerical or experimental effort is required to obtain the response data. One of the main benefits of this method is that typically no model is required for the nonlinearities which enables broad applicability.

More recently, Kerschen et al. [3, 22] developed a method for the calculation of nonlinear modes of conservative large-scale mechanical systems. Their method exploits the periodic nature of nonlinear normal modes and is based on the shooting algorithm in conjunction with time-step integration. Unfortunately, it is not yet clear, whether this method can be extended to dissipative systems.

The periodicity of nonlinear modes in conservative systems is also the starting point for the application of the Harmonic Balance Method (HBM) [23, 24, 25]. The HBM is well-suited for the analysis of strongly nonlinear systems and often

leads to reduced computational effort compared to time integration approaches. Laxalde et al. [26, 8] generalized the HBM to account for the energy decay of the nonlinear mode in dissipative systems. Their modal analysis technique is therefore qualified for the investigation of non-conservative nonlinear systems. Modal properties have also been exploited for the forced response synthesis and the computation of limit-cycle-oscillations. The authors applied the methodology to turbomachinery bladed disks with friction interfaces featuring constant normal load.

The goal of the present paper is twofold. Firstly, a methodology is developed for efficient numerical computation of nonlinear modes of large-scale mechanical systems with generic, including strong and non-smooth, conservative or dissipative nonlinearities, see Section 2. Secondly, nonlinear modal properties are used to accurately calculate forced and self-excited vibrations in Section 3. In Section 4, the proposed methodology is applied to several nonlinear mechanical systems including systems with friction and unilateral contact, and strengths and weaknesses compared to conventional methods are discussed.

## 2. Complex Nonlinear Modal Analysis

The equations of motion of a discrete, time-invariant, autonomous mechanical system can be stated as

$$\mathbf{M}\ddot{\mathbf{u}}(t) + \mathbf{K}\mathbf{u}(t) + \mathbf{g}(\mathbf{u}(t), \dot{\mathbf{u}}(t)) = \mathbf{0}. \quad (1)$$

Herein,  $\mathbf{M} = \mathbf{M}^T > 0$  is the real, symmetric, positive definite mass matrix,  $\mathbf{K} = \mathbf{K}^T$  is the real, symmetric stiffness matrix and  $\mathbf{u}(t)$  is the vector of generalized coordinates. The vector  $\mathbf{g}$  can comprise linear and nonlinear functions dependent on displacement and velocity. Without loss of generality, the generalized coordinates of the system can be defined in such a way that  $\mathbf{u}(t) = \mathbf{0}$  is an equilibrium point and  $\mathbf{K}$  contains the symmetric part of the linearization of  $\mathbf{g}$  with respect to  $\mathbf{u}$  around this equilibrium. The number of DOFs is denoted  $N_{\text{dof}}$ . The restrictions made regarding symmetry of the structure in Eq. (1) are

relaxed in Subsection 2.4. It should be emphasized that the use of generalized coordinates in Eq. (1) explicitly allows preceding component mode synthesis, which can be very useful when treating large-scale structures with localized nonlinearities.

Non-trivial solutions  $\mathbf{u}(t)$  of Eq. (1) are sought in the form of a generalized Fourier ansatz [8],

$$\mathbf{u}(t) = \text{Re}\left\{\sum_{n=0}^{N_h} \mathbf{U}_n e^{n\lambda t}\right\}. \quad (2)$$

Herein,  $\lambda = -D\omega_0 + i\omega_0\sqrt{1-D^2}$  is the complex eigenvalue with the eigenfrequency  $\omega_0$  and the modal damping ratio  $D$ , and  $\mathbf{U}_n$  are vectors of complex amplitudes. The ansatz in Eq. (2) induces the assumption that the damping of the system is frequency-independent [8]. For conservative systems the damping is zero,  $D = 0$ , so that of conservative systems are not affected by this assumption.

If only the first harmonic  $n = 1$  is retained, the ansatz degenerates to the well-known exponential ansatz for damped linear systems. Further, for  $D = 0$  Eq. (2) is completely equivalent to the conventional HBM ansatz for conservative autonomous systems. The damping term  $D$  takes into account the energy decay of the nonlinear mode.

Inserting ansatz (2) into Eq. (1) and subsequent Fourier-Galerkin projection with respect to the base functions gives rise to a system of nonlinear algebraic equations,

$$\mathbf{S}_n(\lambda)\mathbf{U}_n + \mathbf{G}_n(\mathbf{U}_0, \dots, \mathbf{U}_{N_h}) = \mathbf{0}, \quad n = 0, \dots, N_h. \quad (3)$$

Capital letters  $\mathbf{U}_n$ ,  $\mathbf{G}_n$  in this equation denote complex amplitudes of the corresponding lower-case time-domain variables.  $\mathbf{S}_n$  are the blocks of the dynamic stiffness matrix,

$$\mathbf{S}_n = (n\lambda)^2\mathbf{M} + \mathbf{K}. \quad (4)$$

### 2.1. Mode normalization

The number of unknowns in Eq. (3) exceeds the number of equations by two. Phase and amplitude normalization have to be performed. In [8], normalization

by prescribed first complex amplitude  $q_m$  and phase  $\phi_m$  of a specified coordinate ‘m’ was proposed,

$$\left|U_1^{(m)}\right| - q_m = 0 \wedge \arg\left(U_1^{(m)}\right) - \phi_m = 0. \quad (5)$$

An amplitude normalization with respect to the kinetic energy facilitates a direct calculation of the frequency-energy-relationship. This is required to resolve modal interactions [27, 3]. The corresponding normalization conditions thus read

$$\frac{1}{T} \int_0^T \frac{1}{2} \dot{\mathbf{u}}^T \mathbf{M} \dot{\mathbf{u}} dt - q_{\text{kin}} = 0 \wedge \arg\left(U_1^{(m)}\right) - \phi_m = 0. \quad (6)$$

For clarity, the time dependence of variables is not denoted here and in the following. The kinetic energy is represented by its mean value on the pseudo-period  $T = \frac{2\pi}{\omega_0}$ . Note that in conjunction with the Fourier ansatz, this integral can be easily evaluated using Parseval’s theorem.

Strong local nonlinearities can induce abrupt changes of the mode shape in the vicinity of the source of nonlinearity, e.g. close to a contact area. If a DOF in such a region is chosen for the amplitude normalization, a weak numerical performance is possible. In contrast, global features such as the kinetic energy typically exhibit a smoother relationship with the modal properties. Therefore, it is expected that the energy normalization can generally improve the computational robustness of the analysis.

The choice of the phase  $\phi_m$  is arbitrary in an autonomous system. A practical reformulation of the generalized phase condition is to simply set the real or the imaginary part of the component to zero.

An appropriate master coordinate must be specified for the phase and amplitude normalization. Note that if  $U_1^{(m)} = 0$ , Eqs. (5) and (6) do not allow a unique normalization of the mode. However, for some types of nonlinearities such as contact constraints, it is generally possible that certain DOF are fully stuck at specific energy levels. In order to avoid this particular situation, it is not recommended to use a nonlinear DOF as master coordinate for the mode normalization in presence of contact. In [12] it is proposed to specify the amplitude

of the linearized mode to be analyzed as master coordinate.

### *2.2. Evaluation of the nonlinear terms*

As in [8], the nonlinear terms  $\mathbf{G}_n$  are integrated on the pseudo-period and therefore the coordinates and forces are treated as periodic within this step, in contrast to the ansatz given by Eq. (2), which takes into account the energy decay. One advantage of this strategy is that classical HBM frameworks do not need to be modified regarding the calculation of  $\mathbf{G}_n$ . In fact, all nonlinear element formulations compatible with the HBM, including time-discrete Alternating-Frequency-Time schemes [28, 29] and event-driven frequency-domain schemes [30, 31], are applicable. In the authors' opinion, however, the major advantage of this strategy lies in the fact that the nonlinear terms are consistent with the steady state in which the nonlinear forces are also periodic. This provides high accuracy for the subsequent synthesis procedure, see Section 3. It has to be investigated whether this strategy induces inaccuracies in case of strongly damped systems. In particular, it should be evaluated whether this strategy for the evaluation of the nonlinear terms leads to a degradation of accuracy in the prediction of transient system behavior.

### *2.3. Condensation of the eigenvalue problem*

In many cases the nonlinear forces  $\mathbf{g}(\mathbf{u}, \dot{\mathbf{u}})$  in Eq. (1) and its Jacobian are highly sparse. By exploiting this sparsity, the computational effort for the modal analysis can be significantly reduced, particularly in case of localized nonlinearities. This strategy has already been followed by several researchers for forced response analysis using the HBM, see e.g. [32, 33, 30, 29]. In this study, it is applied for the first time to the modal analysis of autonomous systems. We propose to consider the spectral decomposition of the linearized system for this task, which is particularly beneficial in this case, as detailed later.

The system of equations (1) can be partitioned with respect to  $N_N$  nonlinear

‘N’ and  $N_L = N_{\text{dof}} - N_N$  linear ‘L’ terms,

$$\mathbf{g} = \begin{bmatrix} \mathbf{g}^N(\mathbf{u}^N) \\ \mathbf{0} \end{bmatrix} \quad \text{with} \quad \mathbf{u} = \begin{bmatrix} \mathbf{u}^N \\ \mathbf{u}^L \end{bmatrix}. \quad (7)$$

Reformulating Eq. (3) accordingly and premultiplying with the dynamic compliance matrix for each harmonic  $n$ ,  $\mathbf{H}_n = \mathbf{S}_n^{-1}$  yields

$$\begin{bmatrix} \mathbf{U}_n^N \\ \mathbf{U}_n^L \end{bmatrix} + \begin{bmatrix} \mathbf{H}_n^{NN} & \mathbf{H}_n^{NL} \\ \mathbf{H}_n^{LN} & \mathbf{H}_n^{LL} \end{bmatrix} \begin{bmatrix} \mathbf{G}_n^N \\ \mathbf{0} \end{bmatrix} = \begin{bmatrix} \mathbf{0} \\ \mathbf{0} \end{bmatrix}, \quad n = 0, \dots, N_h. \quad (8)$$

As the nonlinear forces only depend on the nonlinear unknowns, it is sufficient to solve only the nonlinear part iteratively,

$$\mathbf{U}_n^N + \mathbf{H}_n^{NN} \mathbf{G}_n^N(\mathbf{U}_0^N, \dots, \mathbf{U}_{N_h}^N) = \mathbf{0}, \quad n = 0, \dots, N_h. \quad (9)$$

The dimension of the system of equations in Eq. (3), which is proportional to the number of coordinates of the full system,  $N_{\text{dof}}$ , can therefore be reduced to the dimension of Eq. (9), which is proportional to the number of coordinates associated to nonlinear elements,  $N_N \ll N_{\text{dof}}$ . If required, the remaining DOFs can be easily recovered using  $\mathbf{U}_n^L = -\mathbf{H}_n^{LN} \mathbf{G}_n^N$ . This expansion is required to evaluate the normalization conditions given by Eqs. (5) or (6).

It should be noted that the factorization of the dynamic stiffness matrix has to be computed in each iteration of the nonlinear solver as it depends on the unknown eigenvalue  $\lambda$ . This can in general diminish the advantage of this condensation. Owing to the monomial form of  $\mathbf{S}$  in Eq. (4), however, the inversion can be accomplished very efficiently by using the spectral decomposition of the structural matrices

$$\phi_k^H \mathbf{M} \phi_k = 1, \quad \phi_k^H \mathbf{K} \phi_k = \omega_k^2, \quad k = 1, \dots, N_{\text{dof}}. \quad (10)$$

The expensive matrix inversion can then be restated as a simple matrix product and the trivial inversion of a diagonal matrix,

$$\mathbf{H}_n(\lambda) = \sum_{k=1}^{N_{\text{dof}}} \frac{\phi_k \phi_k^H}{\omega_k^2 + (n\lambda)^2}, \quad n = 0, \dots, N_h. \quad (11)$$

As mentioned in Section 2, the stiffness matrix  $\mathbf{K}$  contains the linear part of the system. The linearized modal basis in Eq. (10) only has to be computed once and for all. It can then be used as a starting guess for the NMA and incorporated in the efficient condensation technique proposed in Eq. (11). The availability of the linearized modes has the additional advantage that the NMA only has to be carried out in the actually nonlinear regime. In fact, it is important to notice that the expression used in Eq. (11) cannot be used in the linear regime since then the denominator corresponding to  $n = 1$  vanishes.

#### *2.4. Extension to systems of general structure*

The proposed method can easily be applied to more general second-order systems, i. e. with linear symmetric and skew-symmetric velocity- and displacement-dependent terms in Eq. (1). The dynamic stiffness matrix in Eq. (4) then has to be augmented accordingly. The spectral decomposition in Eq. (10) is obtained by solving a general, quadratic eigenvalue problem in this case. This decomposition can still be used to assemble the inverse dynamic stiffness matrix in Eq. (11). This decomposition is derived in Appendix Appendix A. It should, however, be noted that linear damping is proposed to be accounted for in the synthesis rather than in the modal analysis, so that it can be varied without re-computation of modal properties, see Section 3.

#### *2.5. Numerical aspects*

The complex eigenvalue problem in Eq. (3) combined with appropriate normalization conditions represents a system of nonlinear algebraic equations, which has to be solved simultaneously within a specified energy range. The result of this solution process are the energy-dependent nonlinear modes, corresponding eigenfrequencies  $\omega_0$  and modal damping ratios  $D$ . Of course, the energy range has to cover the range in which the response of the system is of interest. The synthesis procedure proposed in Section 3 is therefore restricted to the energy range for which the modal properties have been computed.

The resulting system of equations was solved using a Newton-Raphson method.

The eigensolution of the linearized system was taken as an initial guess for a small energy level. In contrast to [8] the solution was continued using a predictor-corrector continuation scheme, see e.g. [34]. This continuation was necessary to compute the complex, multi-valued relationship between the nonlinear modal properties and the energy often reported in this context [27, 3]. It should be noticed that more elaborate bifurcation and stability analysis methods would represent ideal complements to the framework addressed in this study.

The computational efficiency of the solution process was greatly enhanced by providing analytically calculated derivatives of Eqs. (9) and (6) with respect to the unknown harmonic components of the eigenvector and the complex eigenvalue. Analytical derivatives were obtained from manual symbolic differentiation for each type of nonlinearity, as described e.g. in [35]. Automatic differentiation could generally also be used for this task, see [31].

The continuation of the solution generally has to be performed for a large range of the modal amplitude. It is typically not a priori known in what energy ranges the most relevant regimes of the system are. In this study, a logarithmic scaling of the modal amplitude resulted in great computational efficiency in this regard. A linear scaling of the various unknowns (displacement, frequency, damping, energy) was applied in order to obtain approximately matching orders of magnitude, which can have a crucial influence on the convergence behavior of the nonlinear solver.

### 3. Nonlinear modal synthesis

In a linear system, it is possible to formulate the general response as a synthesis of all solutions to the eigenproblem. This synthesis is very efficient owing to the superposition principle and the orthogonality conditions between the modes. In a nonlinear system, however, these relationships do not hold anymore so that further assumptions and restrictions have to be accepted for any type of synthesis procedure. In this study, we restrict the synthesis to the periodic steady-state vibrations of harmonically forced and self-excited systems

and assume the absence of internal resonances. The latter aspect inherently excludes systems which already have multiple eigenvalues in the linear case.

The equation of motion now takes the form

$$\mathbf{M}\ddot{\mathbf{u}} + \mathbf{C}\dot{\mathbf{u}} + \mathbf{K}\mathbf{u} + \mathbf{g}(\mathbf{u}, \dot{\mathbf{u}}) = \text{Re}\{\mathbf{f}_1 e^{i\Omega t}\}. \quad (12)$$

Compared to the autonomous case in Eq. (1), the equation is augmented by a real symmetric viscous damping matrix  $\mathbf{C}$  and a forcing term of complex amplitude  $\mathbf{f}_1$  and frequency  $\Omega$ . This forcing term vanishes in the self-excited setting.

In order to solve Eq. (12) by nonlinear modal synthesis, we apply the single-nonlinear-resonant-mode theory [4]. This theory is based on the observation that in the absence of nonlinear modal interactions, the energy is basically concentrated in a single mode 'j'. This mode dominates the system response and is treated as nonlinear. Owing to their low energy level, the remaining modes are approximated by their linearized counterpart  $\phi_k$  in accordance with Eq. (10). With this assumption, the system response can be formulated as

$$\mathbf{u}(t) \approx \text{Re}\left\{ \underbrace{q_j \sum_{n=0}^{N_h} \psi_n (|q_j|) e^{in\Omega t}}_{\text{nonlinear mode } j} + \underbrace{\sum_{k \neq j}^{N_{\text{dof}}} q_k \phi_k e^{i\Omega t}}_{\text{linearized modes}} \right\}. \quad (13)$$

Herein, the fundamental frequency  $\Omega$  is either the excitation frequency of the harmonic excitation or the frequency of the self-excited vibration,  $\Omega = \omega_j$ . The mode number  $j$  has to be selected so that either the excitation is around the 1 : 1 external resonance of this mode or the self-excitation leads to a limit-cycle-oscillation (LCO) in this mode. A new modal amplitude  $q_j$  and eigenvector with complex amplitudes  $\psi_n$  have been introduced in Eq. (13). The relationship to the variables obtained from the modal analysis is defined as follows:

$$\psi_1^H \mathbf{M} \psi_1 = 1 \quad \Rightarrow \quad q_j \psi_n = \mathbf{U}_n, \quad n = 0, \dots, N_h. \quad (14)$$

For clarity, the formal dependence of  $\omega_j, D, \psi_j$  on  $|q_j|$  is not denoted here and in the following.

Calculation of the modal amplitudes in Eq. (13) is carried out by once again

employing single-nonlinear-resonant-mode theory: The contributions of the linearized modes are calculated in the traditional manner, i. e. by projecting the linearization of Eq. (12) onto the linear part of the modal basis. The modal amplitude of the nonlinear mode is determined independently of the linear modes by projecting the equation of motion formally onto each harmonic  $\boldsymbol{\psi}_n e^{in\Omega t}$  of the nonlinear eigenvector. The fundamental harmonic  $n = 1$  yields

$$\left[ -\Omega^2 + i\Omega\boldsymbol{\psi}_1^H \mathbf{C}\boldsymbol{\psi}_1 + \omega_j^2 + 2D_j\omega_j \quad i\Omega \right] q_j = \boldsymbol{\psi}_1^H \mathbf{f}_1. \quad (15)$$

The last two terms in the brackets correspond to the projection of the stiffness matrix and the nonlinear terms onto the  $j$ -th mode and are readily available from the modal analysis in Section 2.

It can be easily verified that the resulting non-fundamental harmonic equations, i. e. with  $n \neq 1$  essentially give  $\boldsymbol{\psi}_n^H (\mathbf{S}_n \mathbf{U}_n + \mathbf{G}_n) = 0$ , which is inherently fulfilled in accordance with the eigenproblem given by Eq. (3). This applies exactly in case of conservative systems in resonance. For dissipative systems and/or systems driven not precisely at resonance, this approach represents an approximation: Firstly, the dynamic stiffness matrix  $\mathbf{S}_n$  used in Eq. (3) is not identical to the one associated with Eq. (12) in this case. Particularly, it is evaluated at  $\Omega$  rather than at  $\omega_j$ . Similarly, the nonlinear forces are evaluated at the excitation frequency rather than the eigenfrequency. By assuming that these effects can be neglected in the vicinity of the resonance, the multi-harmonic response in Eq. (13) can be synthesized without the need to solve any nonlinear equations in addition to Eq. (15). This is in contrast to [8], where only the fundamental harmonic of the nonlinear mode was considered instead of the multi-harmonic, multi-modal response in Eq. (13). It is conceivable that the accuracy of the approach could generally be increased by overcoming these simplifications, but this would most certainly result in additional computational effort.

Note that  $\boldsymbol{\psi}_1, D_j, \omega_j$  in Eq. (15) depend on the modulus  $|q_j|$  of the complex modal amplitude. Therefore, Eq. (15) must be solved iteratively. Owing to the numerical character of the modal analysis, the modal properties will only be available at discrete amplitude values. Hence, a one-dimensional interpolation

scheme was used in order to apply the continuous formulation in Eq. (15) to the numerical results of the modal analysis described in Section 2. It was found that both piecewise linear and piecewise cubic interpolation schemes performed well in this study.

*Frequency response function synthesis.* The frequency response function (FRF) can be obtained by solving Eq. (15) and employing a continuation on  $\Omega$ . Once the modulus of the modal amplitude  $|q_j|$  has been computed, the phase of the nonlinear modal amplitude is obtained by evaluating Eq. (15). The modal amplitudes of the remaining, linearized modes are also calculated in the traditional manner.

*Backbone curve synthesis.* Often not the whole frequency response function is relevant but only the backbone curve, i. e. the direct relationship between resonance amplitude, resonance frequency and a system parameter. This backbone curve can be obtained from Eq. (15) by setting  $\Omega = \omega_j$  and employing a numerical continuation on the desired system parameter. Similar to the FRF case, the phase and contribution of linearized modes have to be determined to synthesize full response in Eq. (13).

*Calculation of self-excited limit cycles.* In case of self-excited vibrations, the right hand side of Eq. (15) is zero. It directly follows that  $\Omega = \omega_j$  and the equation simplifies to

$$\boldsymbol{\psi}_1^H \mathbf{C} \boldsymbol{\psi}_1 + 2D_j \omega_j = 0. \quad (16)$$

Eq. (16) governs the limit cycle oscillation amplitude  $|q_j|$  of the nonlinear mode. In the self-excited case, the phase is not relevant so that only the modulus needs to be determined. The assumption of a single nonlinear resonant mode implies that the linearized modes must be damped away. Otherwise, they would grow unbounded and/or lead to nonlinear modal interactions, which have been excluded from the synthesis in this study. The full response is thus recovered by the first term in Eq. (13).

### *3.1. Advantages of the proposed nonlinear modal synthesis*

A major benefit of the proposed methodology is that only a scalar nonlinear equation has to be solved for the nonlinear modal amplitude, independent of the number of DOFs originally contained in the system, the type and distribution of nonlinear sources or the number of harmonics in the modal analysis. Hence, the computational effort for the synthesis procedure is almost negligible compared to alternative methods for the computation of the steady state dynamics such as HBM or direct time integration in conjunction with shooting.

It should also be noticed that the approximated response in Eq. (13) is still multi-harmonic and multi-modal in contrast to the approach proposed in [8]. The multi-harmonic character is an important characteristic of the time evolution of the nonlinear forces and the resulting response. The method that we propose here, models this important feature of the solution.

Moreover, the prediction of steady-state vibrations can be carried out in a large range of parameters of the system in Eq. (12), without the need for expensive re-computation of the modal basis. This provides enormous computational savings, in particular for exhaustive parameter variations that are typically required e. g. for uncertainty analysis and optimization.

#### *3.1.1. Variation of the excitation*

Since the nonlinear modes were calculated independent of the excitation force distribution, any force field can be applied to the system. It is only important that the modes have been computed within the energy range, in which the system is driven by the excitation.

This is particularly interesting for applications where the load collective - in terms of spatial distribution and amplitude and phase - is uncertain. Exhaustive parametric studies on the forced response can then be conducted at virtually no extra computational effort.

### 3.1.2. Damping

Although viscous damping was considered initially, other common types of damping can be studied by simply replacing or augmenting the term  $i\Omega\psi_1^H\mathbf{C}\psi_1$  in Eq. (15). For hysteretic damping  $\mathbf{D}_{\text{hyst}}$ , this term results in  $i\psi_1^H\mathbf{D}_{\text{hyst}}\psi_1$ . In case of modal damping  $\eta_j$ , the corresponding term is simply given by  $i\Omega\eta_j$ . Similar to the excitation, damping is often described by uncertain parameters which have to be varied in the design process of industrial applications.

### 3.1.3. Similar parameter sets

In some cases, even parameters of the nonlinear term  $\mathbf{g}(\mathbf{u}, \dot{\mathbf{u}})$  can be varied without re-computation of the nonlinear modal properties. In this study, this is the case for the considered systems in Subsection 4.2-Subsection 4.3 where the only nonlinear terms stem from the preloaded piece-wise linear contact constraints, i. e. the unilateral elastic and the elastic Coulomb contact constraints. It is postulated that the nonlinear dynamic compliance is only dependent on the ratio between preload  $f_{\text{pre}}$  and excitation level  $\|\mathbf{f}_1\|$ . Hence, the response at a different preload  $\tilde{f}_{\text{pre}}$  can be calculated by

$$q_j(\tilde{f}_{\text{pre}}, \mathbf{f}_1) = \frac{\tilde{f}_{\text{pre}}}{f_{\text{pre}}} q_j\left(f_{\text{pre}}, \frac{f_{\text{pre}}}{\tilde{f}_{\text{pre}}} \mathbf{f}_1\right). \quad (17)$$

A strict mathematical proof is beyond the scope of this study. Instead, the performance and accuracy of this hypothesis will be demonstrated in Section 4. It should be noticed that this hypothesis is not required for the general methodology proposed in this study, but it only provides a beneficial feature for the specific contact nonlinearities used in Subsection 4.2-Subsection 4.3.

## 4. Numerical examples

In this section, the nomenclature regarding the nonlinear modes and their interaction is similar to the one used by Kerschen et al. [3]. A  $N : M$  resonance of the  $J$ th mode is denoted as  $\text{SN} : \text{M}, \text{m} = \text{J}$ . If not otherwise specified, the eigenfrequency, i. e. the frequency of the  $1 : 1$  internal resonance is illustrated in

the frequency energy plot for each mode.

In all figures, normalized excitation frequencies  $\Omega^*$  and eigenfrequencies  $\omega_0^*$  are illustrated. The scaling factor is the linearized eigenfrequency of the first mode, unless otherwise specified. Furthermore, response amplitudes  $a^*$  have been non-dimensionalized by scaling with the corresponding linear case.

For investigation of the numerical examples, a predictor-corrector scheme with tangential predictor and pseudo-arc-length parametrization was implemented and used by the authors. For the numerical evaluation of the Fourier coefficients of the nonlinear forces, the well-known time-discrete Alternating-Frequency-Time scheme was employed, see e. g. [36].

#### 4.1. Modal analysis of a system with cubic spring

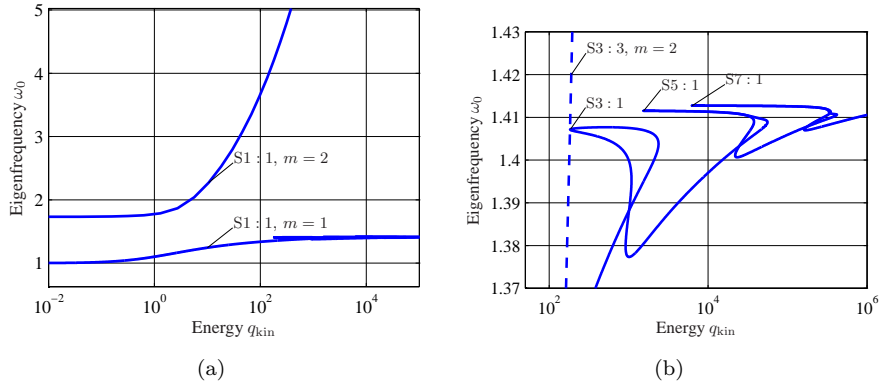


Figure 1: Frequency-Energy-Plot of a 2-DOF system with cubic spring ( (a) overview, (b) zoom on the first internal resonances )

As a first validation, the modal analysis technique is first applied to a 2-DOF system with cubic spring thoroughly studied in [3]. The equations of motion read

$$\begin{aligned} \ddot{x}_1 + 2x_1 - x_2 + 0.5x_1^3 &= 0 \\ \ddot{x}_2 - x_1 + 2x_2 &= 0. \end{aligned} \quad (18)$$

The frequency-energy plot (FEP) of this system is depicted in Figs. 1a- 1b. The system basically has two eigenfrequencies corresponding to the in-phase  $m = 1$

and out-of-phase  $m = 2$  mode. The stiffening behavior of the cubic spring becomes apparent.

Internal resonances occur when the eigenfrequencies of the two modes are commensurable at the same energy level. This happens despite the fact that the linearized eigenfrequencies are not commensurable, because of the general frequency-dependence of each mode. The 3:1, 5:1 and 7:1 internal resonances between the modes are illustrated in Fig. 1b. At the tip of the ‘tongues’, the first eigenfrequency is precisely  $\frac{1}{3}$ ,  $\frac{1}{5}$ ,  $\frac{1}{7}$  of the second eigenfrequency.

In contrast to the time integration scheme in conjunction with a Shooting procedure proposed in [3], the modal analysis technique presented in Section 2 was employed. The results of both methods are fully equivalent. Several harmonics have to be retained in the multi-harmonic expansion in order to accurately resolve the internal resonances. A more detailed bifurcation and stability analysis of the nonlinear modal interactions was considered beyond the scope of this paper. The interested reader will find a detailed analysis of this system is presented in [3].

#### 4.2. Analysis of a clamped beam

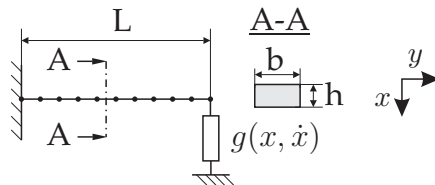


Figure 2: Clamped beam with nonlinear element

The clamped beam as depicted in Fig. 2 was investigated. Its specifications are: Size  $L = 200$  mm,  $b = 40$  mm,  $h = 3$  mm, Young’s modulus  $E = 210,000$  MPa and density  $\rho = 7800 \frac{\text{kg}}{\text{m}^3}$ . The beam was discretized by ten Euler-Bernoulli beam elements, the displacement was constrained to the transverse ( $x$ ) direction. The beam is connected to nonlinear force elements at its free end. Different types of nonlinearity  $g(x, \dot{x})$  will be investigated with respect to their effect on

the overall vibration behavior of the system. In the following, the response amplitude  $a$  is defined as the maximum value of the zero-mean tip displacement.

#### 4.2.1. Unilateral spring nonlinearity

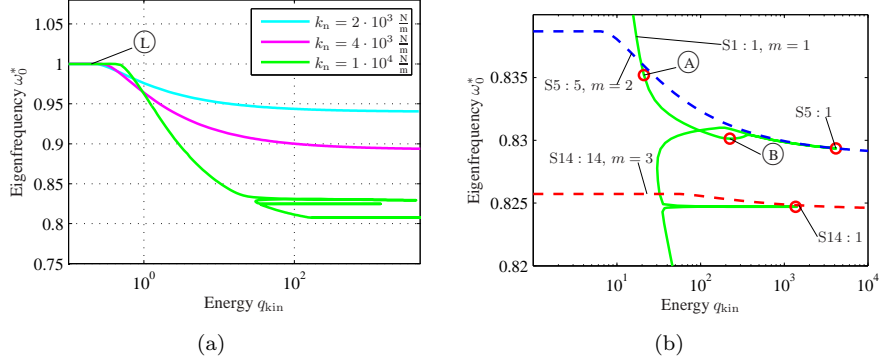


Figure 3: Frequency-Energy-Plot of a clamped beam with unilateral preloaded spring ( (a) overview for different normal stiffness values, (b) zoom on the first internal resonances for  $k_n = 1 \cdot 10^4 \frac{\text{N}}{\text{m}}$  )

First, a unilateral spring with stiffness  $k_n$  will be considered,

$$g(x, \dot{x}) = k_n (x + a_0)_+ . \quad (19)$$

The value in the parenthesis is only considered if it is greater than zero. Note that the spring is preloaded by a compression of length  $a_0$ .

The frequency-energy-plot of the first bending mode is depicted in Figs. 3a-3b. For low energies, the system exhibits linear behavior, i. e. the eigenfrequency remains constant. Once the vibration amplitude is large enough, there is partial lift-off during the vibration cycle, causing the apparent softening behavior.

In Fig. 3a the spring stiffness value  $k_n$  is varied. The relative frequency shift increases with the spring stiffness. For large stiffness values, e. g.  $k_n = 10^4$ , the system exhibits internal resonances.

The internal resonances are indicated in Fig. 3b. In order to illustrate the modal interactions, the corresponding higher modes  $m = 2, 3$  are also depicted. They are denoted  $N : N$  resonances, where  $N$  is the multiple corresponding to the

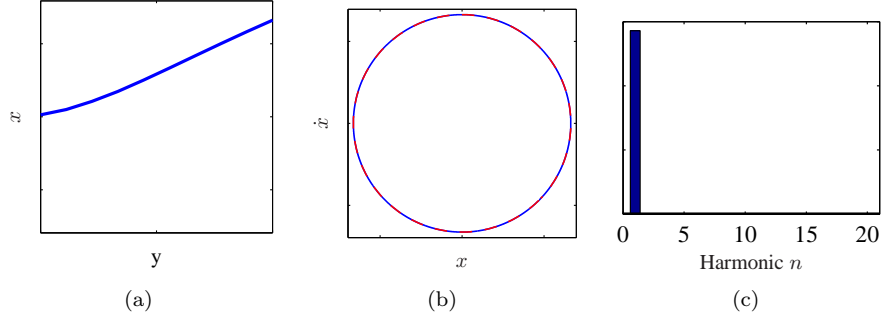


Figure 4: Linear case (L) ( (a) mode shape, (b) phase portrait, (c) frequency content )

$N : 1$  resonance with the first mode. The following two resonance coincidences are presented: A  $5 : 1$  resonance with the second mode and a  $14 : 1$  resonance with the third mode.

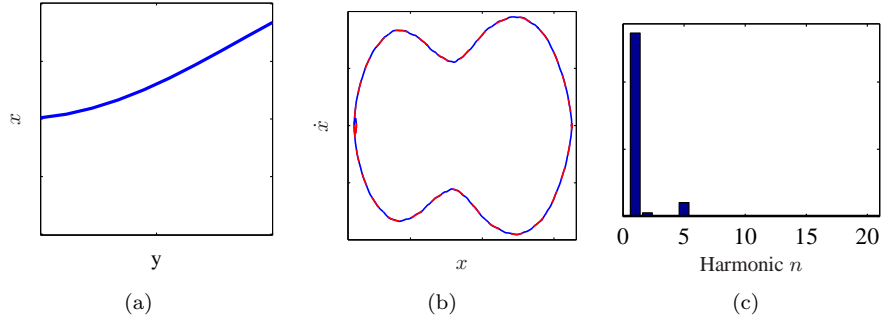


Figure 5: Case (A) ( (a) mode shape, (b) phase portrait, (c) frequency content )

In order to provide a better understanding of the underlying dynamics, the non-linear modes for the points indicated in Figs. 3a-3b are depicted in Figs. 4a-8b. Mode shape, phase portraits for the beam tip deflection and frequency content of the kinetic energy are illustrated. In vicinity of the internal resonance, i. e. at the tip of the tongues, an according higher harmonic content becomes apparent while the frequency content far from these points is dominated by the fundamental harmonic. As it can be deduced from the figures, also the mode shape in the vicinity of these resonances becomes similar to the interacting mode shape.

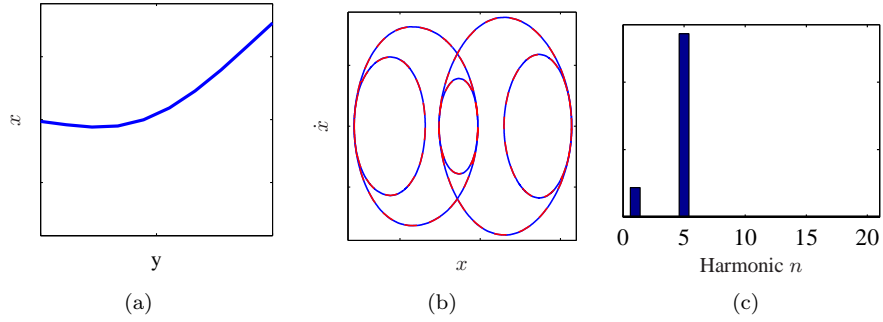


Figure 6: Case (B) ( (a) mode shape, (b) phase portrait, (c) frequency content )

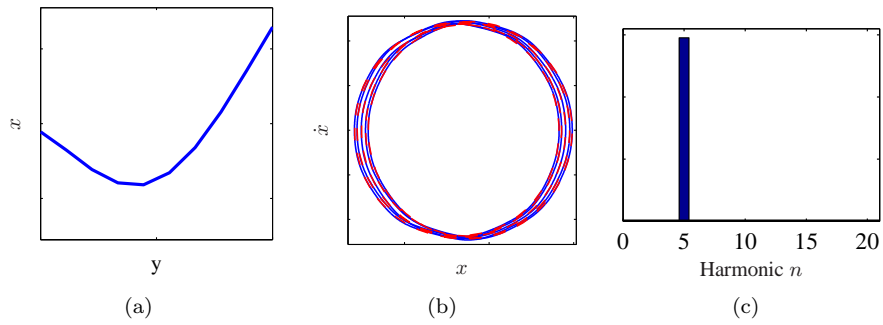


Figure 7: Internal resonance S5:1 ( (a) mode shape, (b) phase portrait, (c) frequency content )

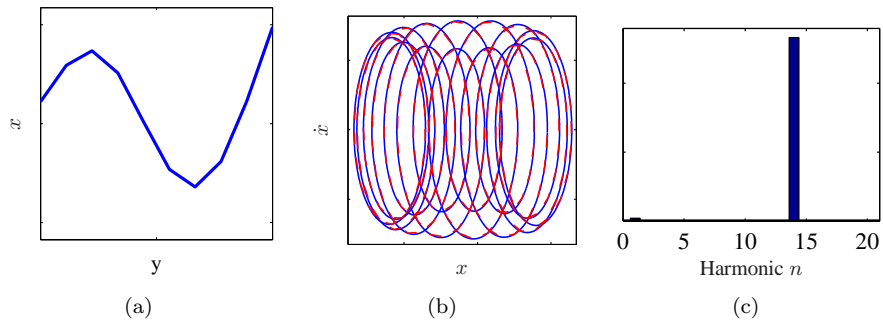


Figure 8: Internal resonance S14:1 ( (a) mode shape, (b) phase portrait, (c) frequency content )

The complex system behavior is well-resolved by the proposed modal analysis technique, which can be ascertained by comparing the phase portrait results of the proposed method (solid) to the time-step integration results (dashed),

cf. Figs. 4b-8b.

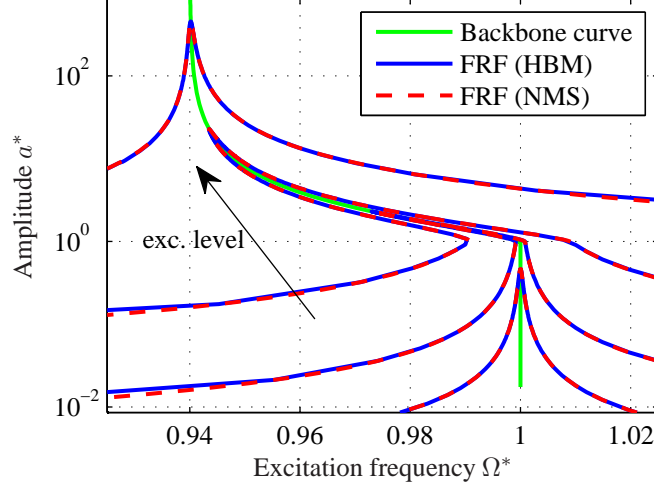


Figure 9: Forced response of a clamped beam with unilateral preloaded spring for varying excitation level

The synthesis method proposed in Section 3 is restricted to regimes where internal resonances are absent. Hence, a value of  $k_n = 2 \cdot 10^3$  was specified for the subsequent investigations. For this value, the forced response to a discrete harmonic excitation at the middle of the beam in Fig. 2 was calculated. The system was excited in a frequency range around the eigenfrequency of the first bending mode. A hysteretic damping  $\mathbf{D}_{\text{hyst}} = \eta \mathbf{K}$  with a damping factor of  $\eta = 0.1\%$  was specified, see Subsection 3.1.2. The results are depicted in Fig. 9. The normalized amplitude is defined as  $a^* = \frac{a}{a_0}$ .

The excitation level has been varied in a wide range. For increasing excitation level the modal amplitude increases and a softening effect becomes apparent, in full accordance with the results in Fig. 3a. Note the overhanging branches resulting in a multi-valued forced response.

The forced response has also been computed with the conventional, multi-term harmonic balance method (HBM) with a harmonic order  $N_h = 7$ . It can be ascertained that the synthesis (NMS) of the forced response is in very good agreement with HBM results. In particular in the vicinity of the resonance, the

accuracy of the proposed synthesis is excellent<sup>1</sup>. Moreover the backbone curve, which has also been directly obtained by the modal synthesis, matches well with the resonances of the forced responses.

#### 4.2.2. Friction nonlinearity

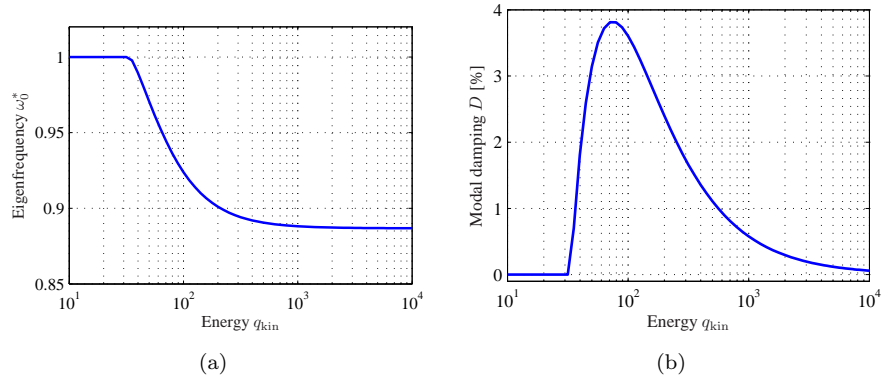


Figure 10: Modal properties of a clamped beam with friction nonlinearity ( (a) eigenfrequency, (b) modal damping )

Next, an elastic Coulomb nonlinearity with a stiffness  $k_t$  and a limiting friction force  $\mu N$  is considered. The expression for the nonlinear force is given by the following differential equation

$$\dot{g}(x, \dot{x}) = \begin{cases} 0 & |g(x, \dot{x})| = \mu N \\ k_t \dot{x} & |g(x, \dot{x})| < \mu N \end{cases}. \quad (20)$$

Several approaches exist for the regularization of this nonlinearity in time and frequency domain [37, 28, 30]. In this study, the time-discretized formulation in [28] was used.

The modal properties are illustrated in Figs. 10a-10b. A softening behavior can be ascertained from the FEP. The modal damping is zero in the fully stuck state. The damping increases to a maximum in the microslip regime and decreases

<sup>1</sup>The expression 'excellent accuracy' was used throughout this study to indicate that relative errors compared to the reference did not exceed 1%.

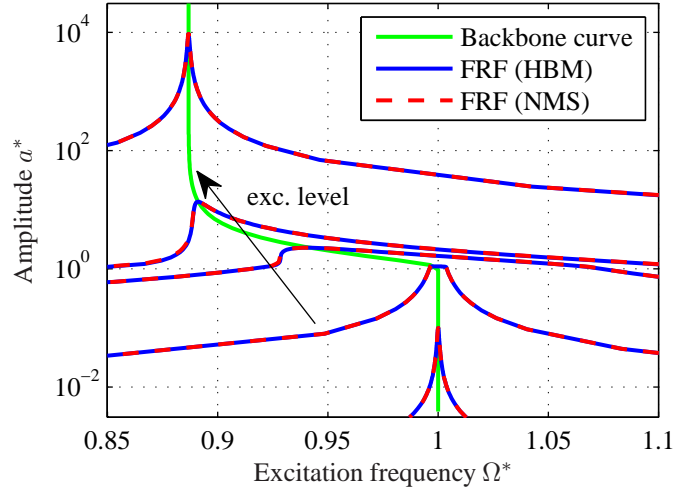


Figure 11: Forced response of a clamped beam with friction nonlinearity for varying excitation level

asymptotically to zero for large energy levels. The decrease of the modal damping ratio may seem counter-intuitive at first, but it can be easily made plausible: For a viscous damping source, the dissipated energy grows quadratically with amplitude, leading to a constant modal damping ratio. The energy dissipated in the Coulomb slider essentially increases only linearly with amplitude, thus leading to a decreasing modal damping for large amplitudes. The interested reader is referred to [38, 8] for further insight in the qualitative dynamic behavior of structures with friction joints.

*Forced response synthesis.* In Fig. 11, the forced response is depicted for a varying excitation level. Again, the results of the proposed synthesis method (NMS) are in excellent agreement with conventional forced response calculations (HBM).

*Calculation of limit cycles.* For the analysis of self-excited vibrations, the viscous damping matrix  $\mathbf{C}$  was defined by inverse modal transformation,

$$\mathbf{C} = \mathbf{\Phi}^{-\text{H}} \mathbf{diag}\{2D_k\omega_k\} \mathbf{\Phi}^{-1}. \quad (21)$$

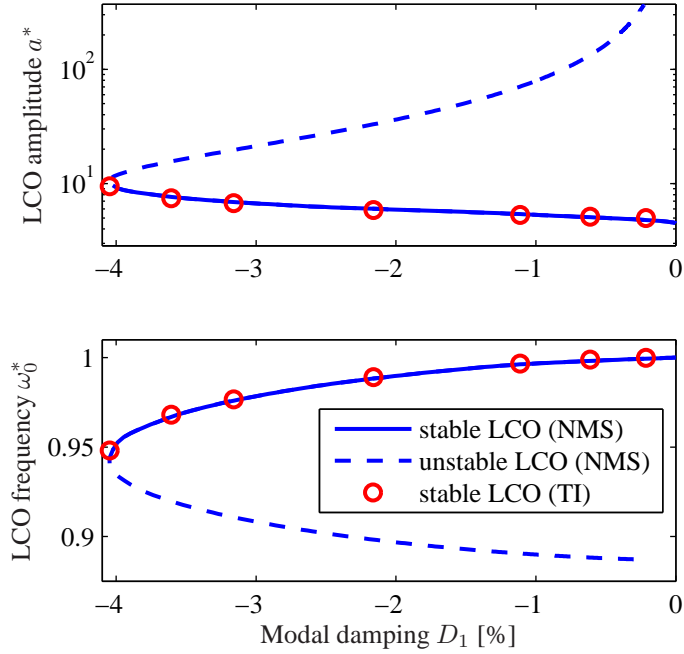


Figure 12: LCO amplitude and frequency w.r.t. modal damping ratio  $D_1$

Herein,  $\Phi = [\phi_1 \ \dots \ \phi_{N_{\text{dof}}}]$  and  $\omega_k$  are the modal matrix and the eigenfrequencies of the linearized system defined in Eq. (10). It should be noted that this damping definition is common for simplified flutter analyses in turbomachinery applications, see e. g. [39]. A negative value was specified for the first modal damping ratio  $D_1$  to obtain self-excited vibrations in the first mode. The remaining damping ratios were defined as  $D_k = 1\%$ ,  $k = 2, \dots, N_{\text{dof}}$ .

In Fig. 12, the LCO amplitude and frequency are illustrated with respect to the modal damping  $D_1$ . Stable and unstable regimes exist. The local stability was determined simply by considering the sign of the slope of the modal damping at the limit cycle amplitude: If the modal damping increases with respect to the amplitude, the limit cycle is stable, otherwise it is not stable. Whether the system reaches a LCO depends on the initial energy in the system. For sufficiently low damping values  $D_1 < -4\%$ , an LCO does not exist, i. e. the modal amplitude would grow unbounded in this case. For positive damping values, the LCO

degenerates to the equilibrium point. It should be noted that the limitation of the vibration amplitude is not only influenced by the amount of nonlinear modal damping, but it also depends on the mode shape, see Eq. (16). The mode shape determines the effective modal damping  $\psi_1^H \mathbf{C} \psi_1$ , assuming a constant damping matrix  $\mathbf{C}$ . The stable LCOs computed by the synthesis (NMS) are in excellent agreement with time-step integration simulations, see Fig. 12.

#### 4.3. Analysis of a turbine bladed disk with shroud contact

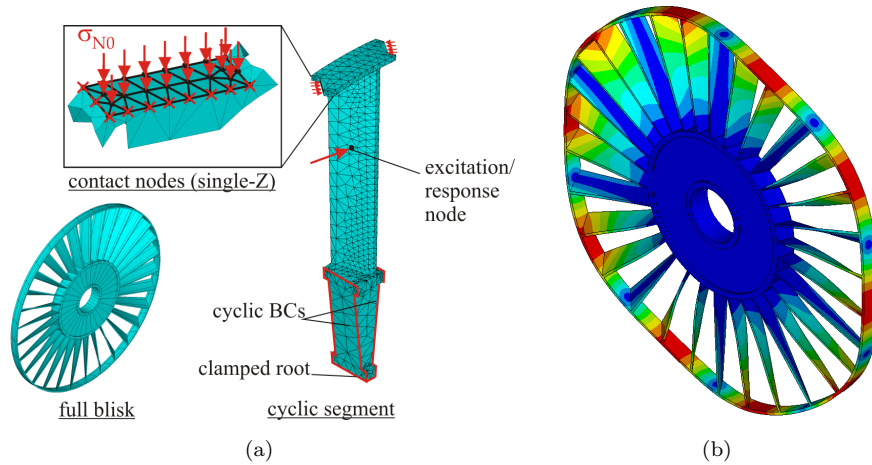


Figure 13: Finite Element Model of a bladed disk with shroud contact ( (a) system definition, (b) investigated mode shape for fixed contact conditions )

In order to demonstrate the applicability of the proposed methodology to more complex systems, a turbine bladed disk with shroud contact interfaces is considered. It comprises 30 blades and is considered to be of perfect cyclic symmetry, cf. Fig. 13a and is similar to the ones investigated in [40, 41, 42]. Owing to the symmetry, only a single sector with cyclic boundary conditions was regarded. The finite element model of the segment consists of 25641 DOFs. A cyclic Craig-Bampton reduced order model [35] of the sector was constructed. Only the DOFs involved in the contact formulation were retained as master coordinates. A number of 50 linear normal modes were ascertained to yield

convergence of the results obtained in this study. The second mode family for a spatial harmonic index 5 was considered in the subsequent investigations, see Fig. 13b. In the forced case, a discrete traveling-wave-type excitation was specified. The amplitude  $a$  is defined as the maximum value of the time domain displacement in the circumferential direction at the response node, cf. Fig. 13a. Impenetrability and friction constraints were enforced in terms of unilateral springs in normal direction and elastic Coulomb elements in the tangential plane [35, 40]. The three-dimensional contact model therefore allows for stick, slip and lift-off phases, and takes into account the influence of the normal dynamics on the stick-slip transitions. The contact constraints were imposed in a node-to-node formulation.

Contact was defined only in the central part of the Z-shaped shroud in this study. It is often desirable to design the normal pressure distribution in such a way that the shroud interfaces are not fully separated during operation so that no high-energy impacts occur and the resonance frequency shifts remains small. Hence, it is regarded as realistic that a portion of the contact area is in permanent contact. For this example, a portion of the nodes was defined as bonded, indicated by crosses in Fig. 13a. A homogeneous normal pressure distribution was specified for the remaining contact area. This specific contact scenario has of course academic character. In order to improve the model accuracy for a realistic case study, a nonlinear static analysis should be carried out, taking into account centrifugal effects on the contact situation and large deformations for the relevant rotational speed range [35].

The modal properties for the bladed disk are depicted in Figs. 14a-14b. The qualitative dependency on the energy is similar to the clamped beam with friction nonlinearity in Figs. 10a-10b. Apparently, several harmonics have to be considered in the multi-harmonic analysis in order to achieve asymptotic behavior of the modal properties due to the highly nonlinear contact constraints. In this case, more harmonics are required for the accurate prediction of the modal damping than for the prediction of the eigenfrequency. Compared to the results in Fig. 10b, the modal damping is less smooth with respect to the

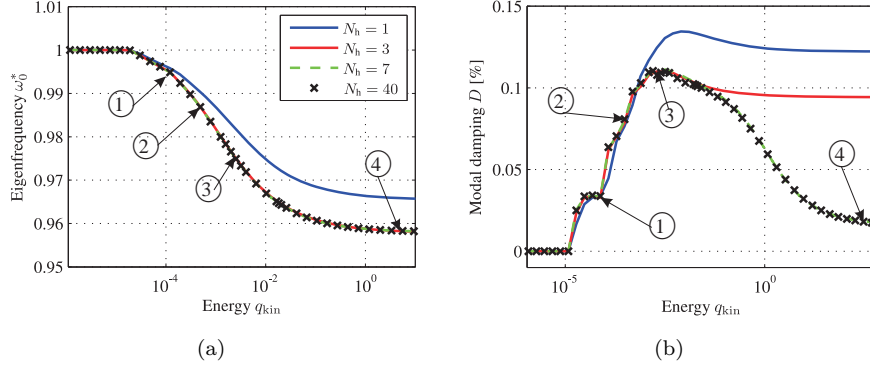


Figure 14: Modal properties of a bladed disk with shroud contact ( (a) eigenfrequency, (b) modal damping )

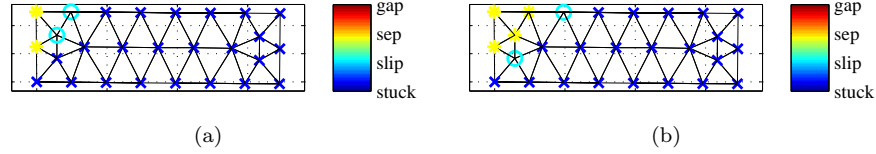


Figure 15: Contact status for different modal amplitudes ( (a) point 1, (b) point 2 )

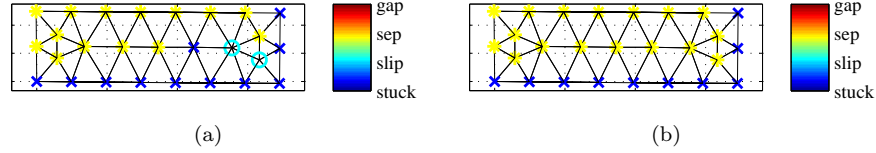


Figure 16: Contact status for different modal amplitudes ( (a) point 3, (b) point 4 )

kinetic energy. The reason for this is that the contact situations change at different energy levels for each contact node, which can be well ascertained from Figs. 15a-16b. For small modal amplitudes, only a small portion of the contact area undergoes stick-slip and partial lift-off. This portion increases with modal amplitude until the entire set of contact nodes undergo stick-slip and lift-off phases during the vibration cycle, except of course for the nodes that were artificially fixed.

The accuracy of the forced response synthesis also depends on the number of

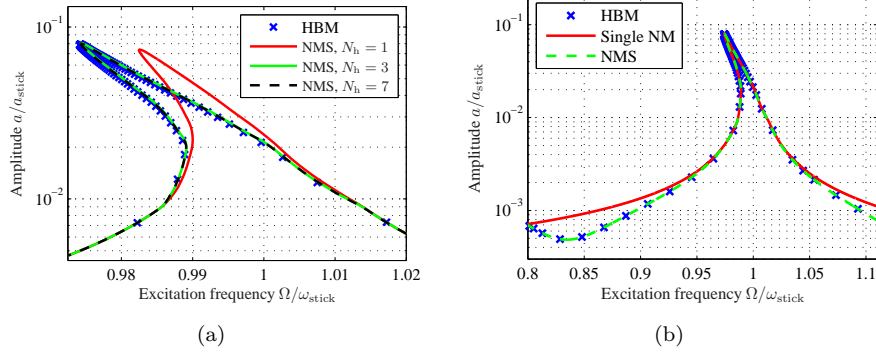


Figure 17: Accuracy of the forced response synthesis ( (a) influence of the number of harmonics  $N_h$  in the modal analysis, (b) influence of the linearized modes )

harmonics  $N_h$  in the modal analysis, see Fig. 17a. A number of  $N_h = 3$  or  $N_h = 7$  should be sufficient to achieve good agreement with the results obtained by the (multi-term) HBM in this case. From the results in Fig. 17b, the effect of the superposition of the linearized mode shapes can be deduced. Particularly in the regime further away from the resonance, the contribution of the linearized modes becomes more significant and should be accounted for. Note that the superposition of the linearized modes is a cheap post-processing calculation and does not significantly increase the computational expense of the numerical investigations.

Finally, the forced response was calculated for varying interlock load  $N$  in the shroud joint, see Fig. 18. Solid lines represent the results obtained by nonlinear modal synthesis, crosses illustrate the results obtained by the multi-term HBM with  $N_h = 7$ . For large values of  $N$ , the shroud is fully stuck. For decreasing normal preload, the resonance amplitude is significantly reduced by means of friction damping up to an optimal preload value  $N^{\text{opt}}$ . The resonance amplitude then increases again. Below a certain value of the normal preload, the system exhibits modal interactions. As a consequence, more than one maximum exists in the forced response. As the assumption of the absence of internal resonances is no longer valid in this case, the prediction by the nonlinear modal synthesis

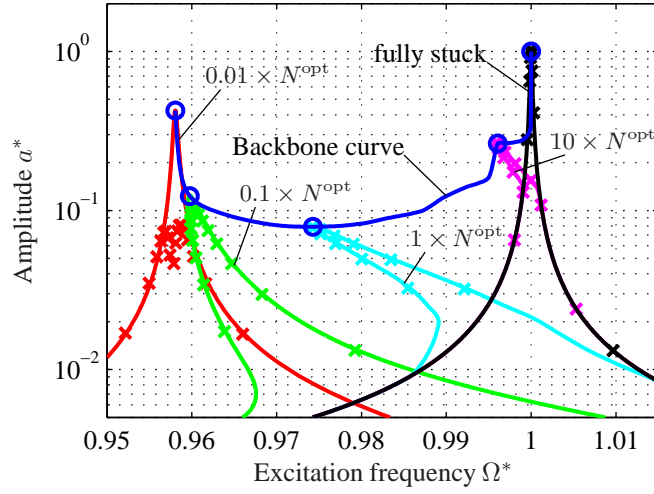


Figure 18: Forced response of a bladed disk with shroud contact for varying interlock load

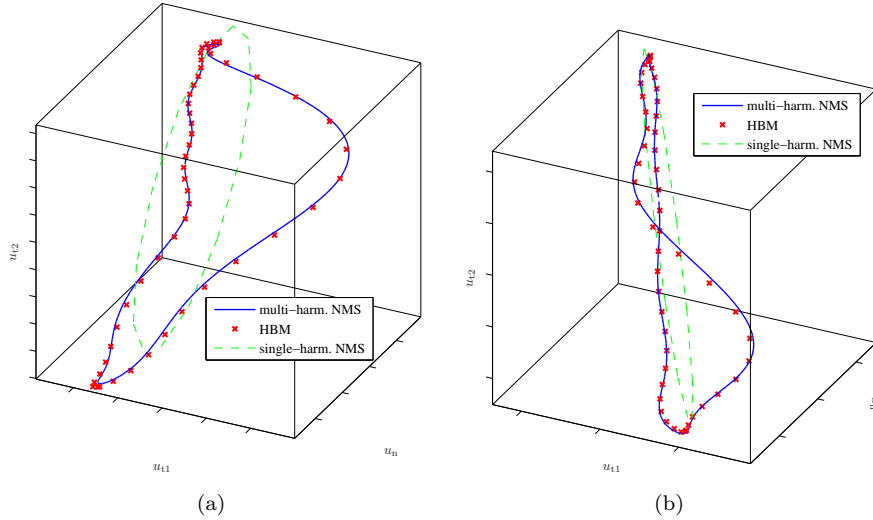


Figure 19: Orbits of upper left contact node at resonance ( ( a)  $0.1 \times N^{\text{opt}}$ , ( b)  $10 \times N^{\text{opt}}$  )

(NMS) fails, cf. the results for  $N = 0.01N^{\text{opt}}$ . The dynamics of the underlying system cannot be approximated with only a single nonlinear coordinate anymore. Up to this regime, however, the prediction of the frequency response function as well as the backbone curve is in excellent agreement with the results obtained from the HBM.

Instead of re-computing the nonlinear modal basis for each value of the interlock load, the forced response was calculated using the similarity hypothesis in Eq. (17). Hence, the modal properties only had to be calculated once to obtain the results in Fig. 18. Regarding the agreement of the results, it can be concluded that the similarity hypothesis was not violated in the considered case.

In Figs. 19a-19b, the orbits of the upper left contact node (see Fig. 13a) at resonance are illustrated. It can be ascertained from the results that the proposed multi-harmonic synthesis significantly increases the accuracy compared to only considering the fundamental harmonic of the nonlinear mode.

In Tab. 1 the computational effort for the forced response analysis of the bladed disk with shroud contact is listed. The effort for the nonlinear modal analysis (NMA) of a single mode is in the order of magnitude of a single frequency response function (FRF) or backbone curve calculation using the conventional multi-harmonic balance method (HBM). It should be noted that this computational effort is strongly related to the number of nonlinear displacement unknowns  $N_{\text{dim}} = (2N_h + 1)N_N = (2 \cdot 7 + 1) \cdot 3 \cdot 17 = 765$  for the 17 three-dimensional contact elements used in this example, see Fig. 13a. Once the modal properties are known, the evaluation of the nonlinear modal synthesis (NMS) has almost negligible computational cost owing to the fact that the number of unknowns is unity, i. e.  $N_{\text{dim}} = 1$ .

Table 1: Computational effort for conventional and proposed methodology

Analysis	$N_{\text{dim}}$	normalized CPU time
FRF (HBM)	765	1.0
Backbone (HBM)	766	0.9
FRF (NMS)	1	< 0.0002
Backbone (NMS)	1	< 0.0002
NMA	767	2.0

## 5. Conclusions

The recently developed complex nonlinear modal analysis technique has been refined in this study. With the extensions, it is now possible to exploit sparsity of the governing algebraic system of equations, making it particularly attractive for systems featuring localized nonlinearities. It was also demonstrated that the use of numerical continuation can facilitate the investigation of modal interactions with this method. Moreover, it was indicated that the approach is closely related to the conventional harmonic balance approaches, so that existing implementations can easily be augmented with only slight modifications.

The resulting nonlinear modal basis was then incorporated into a novel, very compact ROM based on the single-nonlinear-resonant-mode theory. Scalar nonlinear equations have been derived for the calculation of frequency response functions, backbone curves of the forced response and limit-cycle-oscillations. It was shown that system parameters, in particular parameters defining the linear damping and excitation terms can be varied without the need for the comparatively expensive re-computation of the modal basis. The proposed technique can thus be employed to facilitate exhaustive parametric studies on the steady-state vibrations of nonlinear systems.

Numerical examples have shown a broad applicability of the overall methodology. Case studies included large-scale finite element models, strong and non-smooth, conservative and non-conservative nonlinearities. In the absence of modal interactions, the synthesis method showed very good agreement of the multi-modal, multi-harmonic response with results obtained by conventional methods.

Future work on this subject could include the extension of the nonlinear modal synthesis to transient problems arising e. g. in case of dissipative autonomous systems or in presence of transient forcing. Bifurcation and stability analyses are considered as important future developments for the modal analysis technique, in particular to further investigate nonlinear modal interactions. Moreover, it would be desirable to extend the ROM to the treatment of internal resonances

which has already been achieved for the invariant manifold approach. It is conceivable that this could be accomplished similar to [14] by an increase of the number of nonlinear modal amplitudes in modal analysis and synthesis.

## 6. Acknowledgements

The support of Siemens Energy and MTU Aero Engines including the permission to publish this work is kindly acknowledged. The work presented in this paper was funded by AG Turbo 2020; Teilvorhaben 4.1.3, FK 0327719A. The responsibility for the content of the publication rests with the authors.

### Appendix A. Dynamic compliance of a system with general structure

The dynamic compliance matrix is derived for a system with invertible mass matrix  $\mathbf{M}$  but otherwise general structure. The dynamic compliance matrix can be computed blockwise for each harmonic  $n$ . The corresponding dynamic stiffness matrix for the  $n$ th harmonic reads,

$$\mathbf{S}_n(\lambda) = \mathbf{K} + n\lambda\mathbf{C} + (n\lambda)^2\mathbf{M}. \quad (\text{A.1})$$

In order to efficiently compute the dynamic compliance matrix  $\mathbf{H}_n = \mathbf{S}_n^{-1}$ , a spectral decomposition of the state-space matrix  $\mathbf{A}$  of the system,

$$\mathbf{A} = \begin{bmatrix} \mathbf{0} & -\mathbf{I} \\ \mathbf{M}^{-1}\mathbf{K} & \mathbf{M}^{-1}\mathbf{C} \end{bmatrix}, \quad (\text{A.2})$$

is carried out that is defined in analogy to Eq. (10),

$$\mathbf{x}_k^{(l)} \mathbf{A} \mathbf{x}_k^{(r)} = \nu_k, \quad \mathbf{x}_k^{(l)} \mathbf{x}_k^{(r)} = 1, \quad k = 1, \dots, 2N_{\text{dof}}. \quad (\text{A.3})$$

Herein,  $\mathbf{x}_k^{(l)}$ ,  $\mathbf{x}_k^{(r)}$  are left and right eigenvectors associated with the eigenvalue  $\nu_k$ . Uniqueness of the eigenvalues is assumed so that non-identical eigenvectors are orthogonal to  $\mathbf{A}$  and to each other. The eigenvectors can be divided into

two blocks of equal dimensions,

$$\mathbf{x}_k^{(l)} = \begin{bmatrix} \mathbf{v}_k^{(l)} & \mathbf{w}_k^{(l)} \end{bmatrix}, \quad \mathbf{x}_k^{(r)} = \begin{bmatrix} \mathbf{v}_k^{(r)} \\ \mathbf{w}_k^{(r)} \end{bmatrix}. \quad (\text{A.4})$$

With these definitions and some algebraical manipulations, the dynamic compliance matrix can finally be identified as

$$\mathbf{H}_n(\lambda) = \sum_{k=1}^{2N_{\text{dof}}} \frac{\mathbf{v}_k^{(r)} \mathbf{w}_k^{(l)} \mathbf{M}^{-1}}{\nu_k + n\lambda}, \quad n = 0, \dots, N_h. \quad (\text{A.5})$$

Of course, the products  $\mathbf{w}_k^{(l)} \mathbf{M}^{-1}$  can be carried out once and for all prior to the nonlinear dynamic analysis.

## References

- [1] R. M. Rosenberg, Normal Modes of Nonlinear Dual-Mode Systems, *Journal of Applied Mechanics* 27 (1960) 263.
- [2] A. Vakakis, L. Manevitch, Y. Mikhlin, V. Pilipchuk, A. Zevin, *Normal modes and localization in nonlinear systems*, John Wiley & Sons, 2008.
- [3] G. Kerschen, M. Peeters, J. C. Golinval, A. F. Vakakis, Nonlinear normal modes, Part I: A useful framework for the structural dynamicist: Special Issue: Non-linear Structural Dynamics, *Mechanical Systems and Signal Processing* 23 (1) (2009) 170–194.
- [4] W. Szemplinska-Stupnicka, The modified single mode method in the investigations of the resonant vibrations of non-linear systems, *Journal of Sound and Vibration* 63 (4) (1979) 475–489.
- [5] L. Jezequel, C. H. Lamarque, J. Malasoma, Nonlinear modal synthesis based on normal form theory, *Proceedings of the 9th International Modal Analysis Conference, Florence* (1991) 1227–1233.
- [6] Y. H. Chong, M. Imregun, Development and Application of a Nonlinear Modal Analysis Technique for MDOF Systems, *Journal of Vibration and Control* 7 (2) (2000) 167–179.

- [7] C. Gibert, Fitting measured frequency response using non-linear modes, *Mechanical Systems and Signal Processing* 17 (1) (2003) 211–218.
- [8] D. Laxalde, F. Thouverez, Complex non-linear modal analysis for mechanical systems Application to turbomachinery bladings with friction interfaces, *Journal of Sound and Vibration* 322 (4-5) (2009) 1009–1025.
- [9] L. Jezequel, C. H. Lamarque, Analysis of non-linear dynamical systems by the normal form theory, *Journal of Sound and Vibration* 149 (3) (1991) 429–459.
- [10] A. H. Nayfeh, D. T. Mook, *Nonlinear oscillations*, John Wiley & Sons, New York 1979.
- [11] S. W. Shaw, C. Pierre, Normal Modes for Non-Linear Vibratory Systems, *Journal of Sound and Vibration* 164 (1) (1993) 85–124.
- [12] A. H. Nayfeh, *Nonlinear Interactions: Analytical, Computational and Experimental Methods*, John Wiley & Sons, 2000.
- [13] D. Jiang, C. Pierre, S. W. Shaw, Nonlinear normal modes for vibratory systems under harmonic excitation, *Journal of Sound and Vibration* 288 (4-5) (2005) 791–812.
- [14] C. Pierre, D. Jiang, S. W. Shaw, Nonlinear normal modes and their application in structural dynamics, *Mathematical Problems in Engineering* 10847 (2006), 1–15.
- [15] C. Touzé, M. Amabili, Nonlinear normal modes for damped geometrically nonlinear systems: Application to reduced-order modelling of harmonically forced structures, *Journal of Sound and Vibration* 298 (4–5) (2006) 958–981.
- [16] E. Pesheck, C. Pierre, S. W. Shaw, A new galerkin-based approach for accurate non-linear normal modes through invariant manifolds, *Journal of Sound and Vibration* 249 (5) (2002) 971–993.

- [17] D. Jiang, C. Pierre, S. W. Shaw, Large-amplitude non-linear normal modes of piecewise linear systems, *Journal of Sound and Vibration* 272 (3-5) (2004) 869–891.
- [18] G. Kerschen, J.-c. Golinval, A. F. Vakakis, L. A. Bergman, The Method of Proper Orthogonal Decomposition for Dynamical Characterization and Order Reduction of Mechanical Systems: An Overview, *Nonlinear Dynamics* 41 (1) (2005) 147–169.
- [19] Y. P. Zaspá, Nonlinear shapes of steady-state vibrational oscillations of mechanical contact. Symmetrical tangential oscillations, *Journal of Friction and Wear* 28 (1) (2007) 87–104.
- [20] M. Peeters, Theoretical and Experimental Modal Analysis of Nonlinear Vibrating Structures using Nonlinear Normal Modes, Ph.D. thesis, Université de Liège, Liège (2010).
- [21] R. J. Kuether, Allen M. S., Computing Nonlinear Normal Modes Using Numerical Continuation and Force Appropriation, Paper DETC2012-71257, Proc. of ASME 2012 International Design Engineering Technical Conferences & Computers and Information in Engineering Conference (IDETC/CIE 2012), August 12-15, Chicago, USA (2012), 1-12.
- [22] M. Peeters, R. Vigiú, G. Sérandour, G. Kerschen, J. C. Golinval, Nonlinear normal modes, Part II: Toward a practical computation using numerical continuation techniques: Special Issue: Non-linear Structural Dynamics, *Mechanical Systems and Signal Processing* 23 (1) (2009) 195–216.
- [23] A. Y. Leung, Nonlinear modal analysis of frames by the incremental harmonic-balance method, *Dynamics and Stability of Systems* 7 (1) (1992) 43–58.
- [24] P. Ribeiro, M. Petyt, Non-linear free vibration of isotropic plates with internal resonance, *International Journal of Non-Linear Mechanics* 35 (2) (2000) 263–278.

- [25] B. Cochelin, C. Vergez, A high order purely frequency-based harmonic balance formulation for continuation of periodic solutions, *Journal of Sound and Vibration* 324 (1–2) (2009) 243–262.
- [26] D. Laxalde, L. Salles, L. Blanc, F. Thouverez, Non-Linear Modal Analysis for Bladed Disks with Friction Contact Interfaces, Paper GT2008-50860, Proc. of GT2008, ASME Turbo Expo 2008: Power for Land, Sea and Air, June 9-13, Berlin, Germany (2008), 11pp.
- [27] Y. S. Lee, G. Kerschen, A. F. Vakakis, P. Panagopoulos, L. Bergman, D. M. McFarland, Complicated dynamics of a linear oscillator with a light, essentially nonlinear attachment, *Physica D: Nonlinear Phenomena* 204 (1–2) (2005) 41–69.
- [28] J. Guillen, C. Pierre, An Efficient, Hybrid, Frequency-Time Domain Method for the Dynamics of Large-Scale Dry-Friction Damped Structural Systems, Proc. of the IUTAM Symposium held in Munich, Germany, August 3-7 (1998), 1–10.
- [29] S. Nacivet, C. Pierre, F. Thouverez, L. Jezequel, A Dynamic Lagrangian Frequency-Time Method for the Vibration of Dry-Friction-Damped Systems, *Journal of Sound and Vibration* 265 (1) (2003) 201–219.
- [30] E. P. Petrov, D. J. Ewins, Analytical Formulation of Friction Interface Elements for Analysis of Nonlinear Multi-Harmonic Vibrations of Bladed Disks, *Journal of Turbomachinery* 125 (2) (2003) 364–371.
- [31] M. Krack, L. Panning-von Scheidt, J. Wallaschek, A High-Order Harmonic Balance Method for Systems With Distinct States, *Journal of Sound and Vibration* 332 (21) (2013) 5476–5488.
- [32] J. J. Chen, C. H. Menq, Prediction of the Resonant Response of Frictionally Constrained Blade Systems Using Constrained Mode Shapes, Paper 98-GT-548, Proc. of the International Gas Turbine & Aeroengine Congress & Exhibition, Stockholm, Sweden, June 2-5 (1998), 1–10.

- [33] B. D. Yang, J. J. Chen, C. H. Menq, Prediction of Resonant Response of Shrouded Blades With Three-Dimensional Shroud Constraint, *Journal of Engineering for Gas Turbines and Power* 121 (3) (1999) 523–529.
- [34] R. Seydel, *Practical bifurcation and stability analysis: from equilibrium to chaos*, Springer New York, 1994.
- [35] C. Siewert, L. Panning, J. Wallaschek, C. Richter, Multiharmonic Forced Response Analysis of a Turbine Blading Coupled by Nonlinear Contact Forces, *Journal of Engineering for Gas Turbines and Power* 132 (8) (2010) 082501–082509.
- [36] T. M. Cameron, J. H. Griffin, An Alternating Frequency/Time Domain Method for Calculating the Steady-State Response of Nonlinear Dynamic Systems, *Journal of Applied Mechanics* 56 (1) (1989) 149–154.
- [37] B. D. Yang, C. H. Menq, Characterization of 3D Contact Kinematics and Prediction of Resonant Response of Structures Having 3D Frictional Constraint, *Journal of Sound and Vibration* 217 (5) (1998) 909–925.
- [38] K. Popp, L. Panning, W. Sextro, Vibration Damping by Friction Forces: Theory and Applications, *Journal of Vibration and Control* 9 (3-4) (2003) 419–448.
- [39] E. P. Petrov, Analysis of Flutter-Induced Limit Cycle Oscillations in Gas-Turbine Structures With Friction, Gap, and Other Nonlinear Contact Interfaces, *Journal of Turbomachinery* 134 (6) (2012) 061018–13.
- [40] M. Krack, L. Panning-von Scheidt, J. Wallaschek, C. Siewert, A. Hartung, Robust Design of Friction Interfaces of Bladed Disks With Respect to Parameter Uncertainties, Paper GT2012-68578, *Proc. of ASME Turbo Expo 2012*, June 11-15, Copenhagen, Denmark (2012), 1–12.
- [41] M. Krack, L. Panning-von Scheidt, C. Siewert, A. Hartung, J. Wallaschek, Analysis and Robust Design of Friction Joints for Vibration Reduction

in Bladed Disks, Paper-ID 224, Proc. of SIRM 2013 – 10th International Conference on Vibrations in Rotating Machines, February 25-27, Berlin, Germany (2013), 11pp.

- [42] M. Krack, L. Panning-von Scheidt, J. Wallaschek, A. Hartung, C. Siewert, Reduced Order Modeling Based on Complex Nonlinear Modal Analysis and its Application to Bladed Disks With Shroud Contact, Paper GT2013-94560, Proc. of ASME Turbo Expo 2013, June 3-7, San Antonio, TX, USA (2013), 1–11.